*Article*

# Effect of HPT on the First Hydrogenation of LaNi$_5$ Metal Hydride

**Renato Belli Strozi** [1,2] , **Julia Ivanisenko** [3] , **Natalia Koudriachova** [4] **and Jacques Huot** [2,*]

[1] Graduate Program of Materials Science and Engineering, Federal University of Sao Carlos, Rod. Washington Luis, km 235, Sao Carlos 13565-905, SP, Brazil; renato.strozi@irh.ca

[2] Hydrogen Research Institute, Université du Québec à Trois-Rivières (UQTR), Trois-Rivieres, QC G9A 5H7, Canada

[3] Institute of Nanotechnology (INT), Karlsruhe Institute of Technology (KIT), 76021 Karlsruhe, Germany; julia.ivanisenko@kit.edu

[4] School of Physical Sciences, University of Cambridge, Trinity Lane, Cambridge CB2 1TN, UK; nkudriashova@outlook.com

[*] Correspondence: jacques.huot@uqtr.ca

**Abstract:** This paper reports the effect of high-pressure torsion (HPT) on the first hydrogenation of LaNi$_5$. We found that, for loose powder, reduction of particle size has an effect of increasing the incubation time and decreasing the hydrogen capacity. A higher amount of HPT turns only marginally reduce the incubation time but has no effect on hydrogen capacity. In all cases, the first dehydrogenation and subsequent hydrogenation have the same kinetics, irrespective of the particle size or number of HPT turns. Therefore, for LaNi$_5$, HPT has a beneficial effect only for the first hydrogenation.

**Keywords:** hydrogen storage; high-pressure torsion; AB$_5$ alloys; LaNi$_5$

## 1. Introduction

Hydrogen is a key energy vector, especially for renewable energies. For a broad utilization of hydrogen, a suitable means of storage should be available. Presently, hydrogen storage in gaseous (high pressure) and liquid states are the main methods used in commercial applications. However, these techniques have limitations in terms of pressure and temperature that makes them not ideally suitable for certain uses. Metal hydrides can store hydrogen at low temperature and pressure with a high volumetric density. The main disadvantage is the low gravimetric density. There are many types of metal hydrides such as AB$_2$, AB$_5$, Mg-based, TiFe, etc. where A is a hydride-forming element and B is a non-hydride-forming element.

Magnesium-based alloys have been intensively studied because of their high hydrogen storage capacity. Many different magnesium-based systems are considered such as ternary hydrides (Mg$_2$FeH$_6$, Mg$_2$CoH$_5$, Mg$_2$NiH$_4$), nanocrystalline, additives, etc. However, there are still many unknown factors that influence the hydrogenation/dehydrogenation of magnesium-based alloys [1]. Magnesium and magnesium alloys were one of the first materials to have been studied for the effect of HPT technique to improve hydrogen storage properties [2–6].

Despite its relatively low hydrogen storage capacity (1.86 wt.%), the alloy TiFe is still considered for practical applications because of its relatively low cost and the fact that it can operate close to room temperature [7]. The alloys of type A$_x$B$_y$ have a large range of hydrogen capacity and temperature of operation depending on the stoichiometry and constituent elements. A short review of these alloys has been written by Lys et al. [8]. The present state-of-the-art of metal hydrides is given in a recent review paper by Hirscher et al. [9]. Processing hard and brittle materials as TiFe by HPT can be challenging, but it has been successfully shown that it is beneficial for activation and air resistance [10–13].

The classic representative of $AB_5$ alloys is $LaNi_5$. It absorbs hydrogen at room temperature and has a relatively low hydrogen capacity of about 1.5 wt.%. However, to be marketable, metal hydrides should also have low cost. It is important to realize that cost should include the raw materials but also the synthesis process of the hydride.

It is a common feature of metal hydrides that the first hydrogenation (also called activation) of the as-synthesized alloy is difficult, needing high temperature and hydrogen pressure [14,15]. This adds to the cost of metal hydrides and may make it non-competitive with other hydrogen storage methods. Therefore, a solution to this problem should be found.

In a previous investigation, we have shown that cold rolling of $LaNi_5$ is beneficial for the first hydrogenation of the alloy [16]. The exact mechanism for such improvement is still not fully understood. Clearly, nanocrystallinity plays a role, but as nanocrystalline ball-milled samples did not show a similar improvement, other factors should be involved.

High-pressure torsion (HPT) is a technique in which a thin disk is inserted between two Bridgman-type anvils and subjected to torsional straining under a high hydrostatic pressure [17,18]. In the synthesis of materials by HPT, a high shear strain could be reached, resulting in nanostructured alloys with high density of lattice defects, which can improve the hydrogen diffusion and would be beneficial to improving the hydrogen activation of metal hydrides [10,19,20]. Moreover, as described by Yamamoto et al. the $LaNi_5$ is brittle under uniaxial compression, resulting in the introduction of cracks associated with the introduction of dislocations, which contributes to reducing the absorption equilibrium pressure between the first and second cycles [21].

As we saw in our previous experiment, cold rolling of $LaNi_5$ resulted mainly in reducing the particles size and agglomeration in a small plate. By performing the same investigation with HPT, we want to explore the effect of high strain on the first hydrogenation of $LaNi_5$.

## 2. Materials and Methods

Commercial $LaNi_5$ powder purchased from Whole Win (Beijing, China) Materials Sci. & Tech. Co., Ltd. was used. The cast alloy was first reduced in powder using an agate mortar and pestle. To study the effect of particle size, the as-crushed powder was sieved to obtain three different distributions: particles of more than 1 mm diameter ($p > 1$); particles between 0.5 and 1 mm diameter ($1 > p > 0.5$) and particles smaller than 0.5 mm ($p < 0.5$). For HPT tests, the as-crushed powder was sieved to a particle size $p < 0.5$ and pressed into a disk of 10 mm diameter and about 1 mm thick under a pressure of 1 GPa (HPT0). The as-obtained pellets were processed by HPT at 5 GPa for 1, 3 and 5 turns (HPT1, HPT3 and HPT5, respectively).

The hydrogen absorption and desorption kinetic curves were measured with a home-made Sieverts-type apparatus. All measurements were performed at 323 K with a hydrogen pressure of 1500 kPa for absorption and 5 kPa for desorption. As the hydrogen absorption/desorption is measured by the change of pressure, the pressure at the end of the measurement is different than at the beginning. For absorption, this is not a real problem because the pressure drop is small enough in order for the pressure always to be above the plateau pressure. The problem is in desorption. For desorption, we used a supplementary volume of 1000 cc in order to reduce the pressure increases. Still, typically, the pressure increased to about 25 kPa. For stable hydrides, this may mean that the desorption plateau pressure was reached, and the reaction stopped without the sample being totally desorbed.

Desorption at 100 kPa is more suitable for practical applications, but for testing the effectiveness of HPT on sorption properties, we found that working at 5 kPa permitted faster kinetics and easier comparison. The crystal structure was analyzed from X-ray powder diffraction patterns registered on a Bruker D8 Focus apparatus (Billerica, MA, USA) with CuKα radiation. The crystallite size, lattice parameters and microstrains were evaluated with the Rietveld refinement method using the Topas software via the fundamental parameters approach [22].

## 3. Results

### 3.1. Crystal Structure of As-Processed Alloys

The alloy LaNi$_5$ crystallizes in the hexagonal space group P6/mmm and *Haucke* CaCu$_5$ prototype. A recent paper by Joubert et al. discusses the structure and properties of this compound [23]. Figure 1 shows the diffraction patterns of the LaNi$_5$ in powder form (powder) and after being pressed in a pellet before the HPT test (HPT0). It also shows the diffraction patterns of the pellets after 1, 3 and 5 turns (HPT1, HPT3 and HPT5).
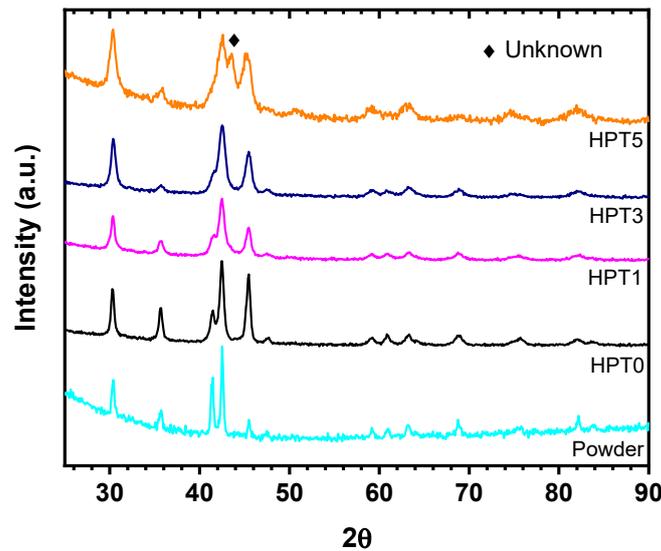


**Figure 1.** X-ray diffraction patterns of LaNi$_5$ at various stages: as-received powder (Powder), pressed pellet (HPT0) and pellet after 1, 3 and 5 HPT turns (HPT1, HPT3 and HPT5). The vertical lines indicate the position of LaNi$_5$ Bragg peaks.

From Figure 1, we see that, up to 3 HPT turns, the patterns are single-phase LaNi$_5$ with broadening of the peaks with HPT. However, for 5 turns (HPT5), there is the appearance of a broad peak at 43.5°. Moreover, the relative intensity of the (2–100,000) peak at 35.7° decreases with the number of HPT turns, except maybe for the HPT5 pattern, where the intensity seems to slightly increase. To precisely determine the crystal structure parameters, a Rietveld refinement was performed on each pattern. The results are presented in Table 1. The lattice parameters of LaNi$_5$ reported in the literature varies in a wide range, moving from $a$ = 5.149 Å, $c$ = 3.621 Å [24] to $a$ = 5.0033 Å, $c$ = 3.9820 Å [25].

**Table 1.** Results of Rietveld refinements of the patterns displayed in Figure 1. $a$ and $c$ are the lattice parameters of the LaNi$_5$ unit cell (space group P6/mmm). Vol is the unit cell volume, $\tau$ is the crystallite size and $\varepsilon$ is the microstrain. Error on the last significant digit is indicated in parentheses.

| Sample | $a$ (Å) | $c$ (Å) | Vol (Å$^3$) | $\tau$ (nm) | $\varepsilon$ (%) |
|---|---|---|---|---|---|
| Powder | 5.027 (1) | 3.977 (1) | 86.85 (3) | 34 (5) | 0.11 (1) |
| HPT0 | 5.0177 (8) | 3.9832 (6) | 86.85 (3) | 17.7 (6) | 0.15 (1) |
| HPT1 | 5.019 (1) | 3.986 (1) | 86.96 (5) | 10.2 (3) | 0.12 (2) |
| HPT3 | 5.025 (1) | 3.9921 (8) | 87.28 (4) | 12.0 (4) | 0.26 (1) |
| HPT5 | 5.019 (3) | 4.002 (4) | 87.3 (1) | 12 (1) | 0.41 (2) |

From Table 1, we see that the unit cell volume slightly increases with HPT turns. The lattice parameter $a$ does not show a clear trend, but the lattice parameter $c$ slightly increases. The same phenomenon occurs upon ball milling. Joseph et al. reported that upon 100 h of milling LaNi$_5$, the $a$ parameter decreases from 5.0160 Å to 4.975 Å, while the $c$ parameter increases from 3.9836 Å to 4.036 Å [26]. They also observed that the unit cell volume was

slightly smaller after ball milling. In the present case, the unit cell volume increases with HPT but by only about 0.5%.

A decrease of unit cell volume with reduction of particle size has been indicated by Diehm et al. [27]. They showed that, for metals and non-oxide compounds, the decreases of lattice parameters with decreasing particle size are mainly between 0.3% and 3%. This is explained by surface stress. In the present case, the maximum change of *a* and *c* parameters are respectively 0.18% and 0.35%, which is in the same range as reported by Diehm. Therefore, even if in the present case we consider the crystallite size and not the particle size, a similar explanation may be used, i.e., change of surface stress with change of crystallite size.

Table 1 also indicates that HPT leads to a reduction of crystallite size ($\tau$) and an increase of microstrains ($\varepsilon$). These explain the broadening of the peaks with HPT. Most of the crystallite size reduction is due to pressing (HPT0). Turning further reduces the crystallite size, but it seems there is a lower limit of about 10 nm. Microstrain has a different behavior. Pressing and one HPT turn does not change the microstrain value, but additional turning increases it. However, the crystallite size measured by XRD is the size of coherently scattered domains, i.e., areas with a perfect crystallite lattice slightly misoriented from each other, whereas grains are delineated by high angle grain boundaries.

In the Rietveld refinement of pattern HPT5, there is a peak at 43.5°. From this refinement, we fitted this single peak and obtained full width at half maximum (FWHM) of about 1°. This seems to be too narrow to be considered as an amorphous phase. The nature and origin of this peak is still unclear. It may be contamination, or a phase transition but, as only one Bragg peak is present, it is difficult to identify the nature of this peak. Nevertheless, this peak represents about 16% of the pattern, according to Rietveld refinement.

### 3.2. First Hydrogenation and Dehydrogenation

The effect of particle size on the first hydrogenation and dehydrogenation kinetics was investigated by sieving the hand crushed ingot in three different populations: particles bigger than 1 mm ($p > 1$); particles with size between 0.5 and 1 mm ($1 > p > 0.5$) and particles smaller than 0.5 mm ($p < 0.5$). Figure 2 shows the first hydrogenation kinetics at room temperature under 1500 kPa of hydrogen for the different particle size of the raw powder. The most remarkable fact is that the incubation time increases with decreasing particle size. This is counterintuitive, as one expects the kinetics to be faster for smaller particle size because of the larger specific surface area. The incubation time for the $p < 0.5$ distribution is ten times bigger than for the $p > 1$ population. Moreover, kinetics at half capacity (tangent of the slope) is three times faster for the $p > 1$ population compared to the $p < 0.5$ population.

The maximum capacity decreases with decreasing particle size: The $p > 1$ population has a maximum capacity of 1.50 wt.%, while the ($1 > p > 0.5$) and ($p < 0.5$) populations respectively have capacities of 1.40 wt.% and 1.32 wt.%. A possible explanation of this decrease may be the presence of surface oxide. It is well known that, on the surface of $LaNi_5$, there is segregation due to a difference in the surface energy of the alloy components [28–31]. This results in a coating of $La_2O_3$ or $La(OH)_3$ with a thin surface layer of NiO. Under hydrogen, the NiO is reduced, and nickel then acts as an active cluster for the decomposition of $H_2$ molecules. Litvinov et al. estimated the thickness of oxide to be of the order of one dozen monolayers [31]. However, the oxide was formed under controlled mild conditions (room temperature ($3.3 \times 10^{-4}$ Pa of oxygen for 45 s). In the present investigation, we expect that the surface oxide will be much thicker. If one considers that the oxide thickness is the same for all distributions and that the oxide forms a uniform shell around the particle, then the ratio of the loss capacity over the total theoretical capacity (1.5 wt.%) is given by $3\Delta/r$, where $\Delta$ is the oxide thickness and r is the particle's radius. Using this formula, we estimated the oxide thickness to be around 20 μm. However, at this moment, we have no hard evidence of the presence, or lack of, of an oxide layer. Still, the main problem is to explain the short incubation time for the bigger particles.
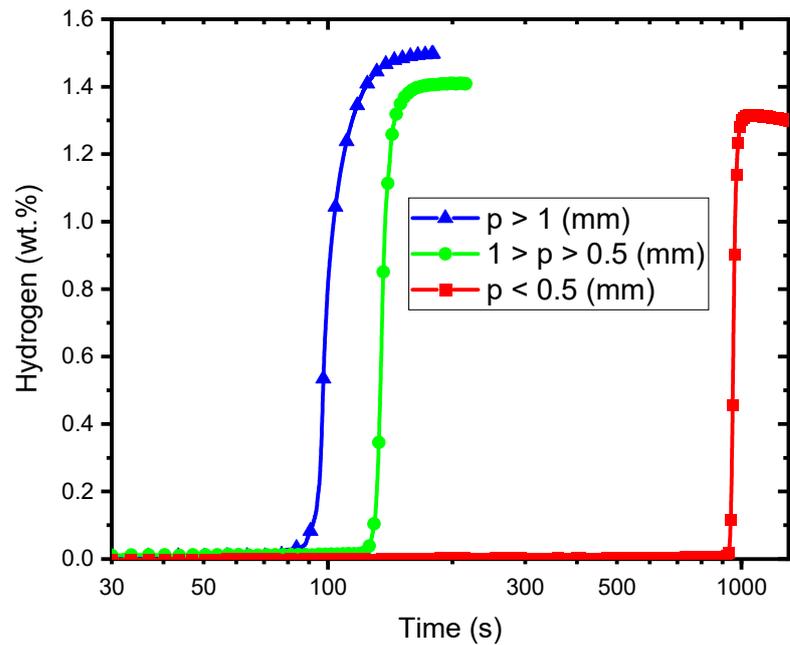
**Figure 2.** First hydrogenation at room temperature under 1500 kPa of hydrogen of LaNi$_5$ for different particle sizes.

Figure 3 shows the first dehydrogenation of samples with various particle sizes. We see that the kinetic does not depend on particle size and that all samples fully desorbed in 14 min. Similar results were observed in a previous investigation on the effect of ball milling and cold working of LaNi$_5$ [16]. Important differences were observed for the first activation, but all samples presented the same first dehydrogenation kinetics. In addition, the second hydrogenation kinetic was the same for all samples and was quite fast, reaching full capacity in less than 2 min. As the difference between samples is seen only for the activation, the second cycle is not discussed here.
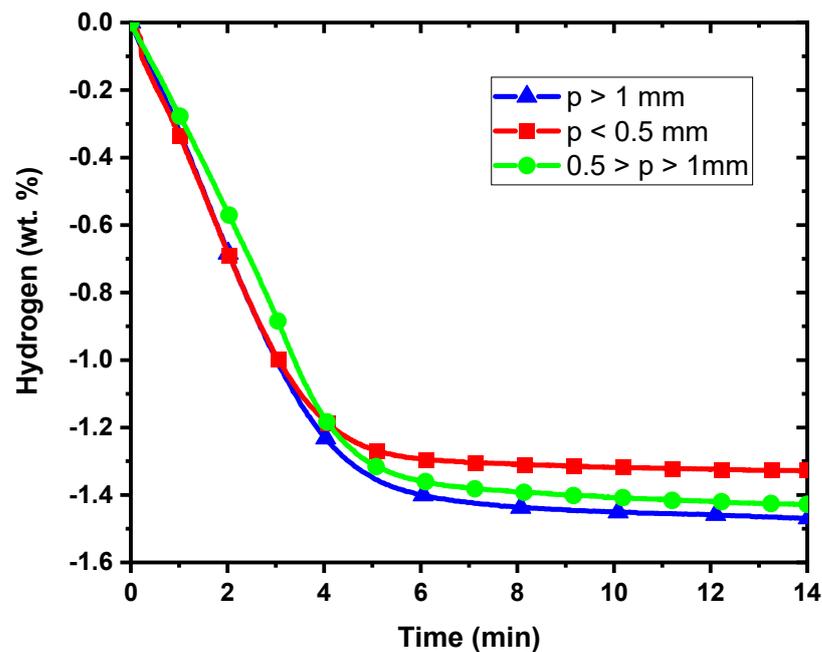


**Figure 3.** First dehydrogenation at room temperature under partial vacuum of as-cast alloy with different particle sizes.

Figure 4 shows the first hydrogenation after HPT for a different number of turns. The sample HPT0 has only been subjected to high pressure (no torsion). To create this sample, powder with small particle size was used ($p < 0.5$ mm). The incubation time for this distribution was about 1000 min (see Figure 2), while the incubation time for HPT0 was 90 min, an order of magnitude smaller. The incubation time for the ($p > 1$ mm) distribution was 93 min, which was practically the same as HPT0. It has been shown that intermetallic LaNi$_5$ under uniaxial compression results in cracks and high-density of defects, especially edge dislocations [21,32]. These features can explain the reduction of the incubation time in the case of the HPT's samples. However, reduction of incubation time for the big particles was due to another characteristic. One possibility is that the short incubation time might have been due in part to the good thermal contact either within a particle ($p > 1$ mm) or between particles, such as in HPT0. Thus, we could argue that high pressure alone may not be as efficient to induce cracks and defects. We see that for HPT1, HPT3 and HPT5, the incubation time dropped to 30 min for the HPT1, a factor of three smaller than the HPT0 time. This is clear proof that HPT is efficient in inducing cracks and defects. Further torsion only reduced the incubation time to 28 min for HPT3 and 21 min for HPT5. Still, the main effect of HPT is seen for the first turn. All samples absorbed the full capacity. Therefore, HPT does not have any detrimental effect in terms of hydrogen capacity.
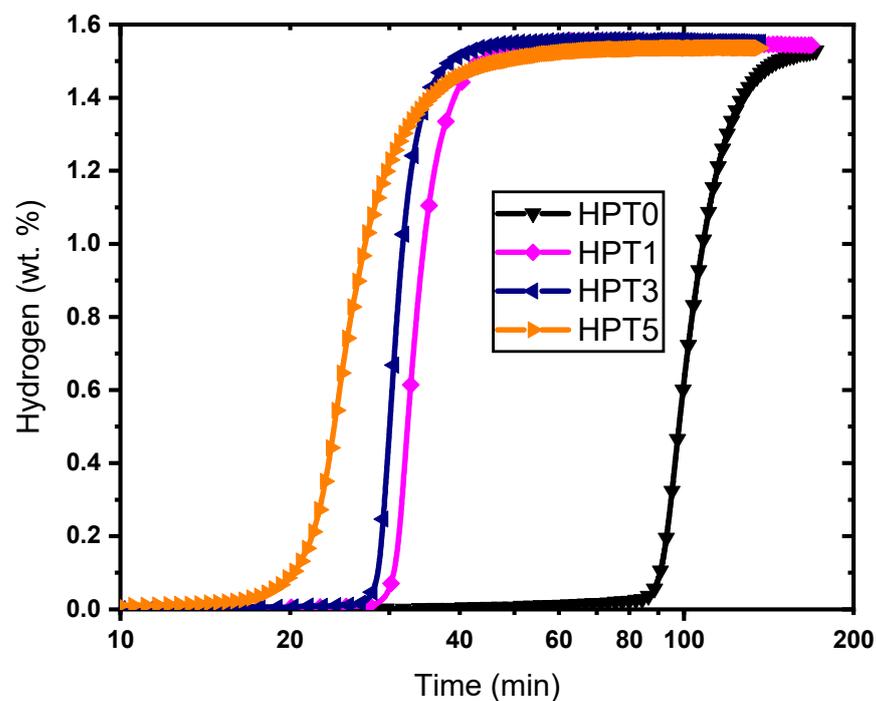


**Figure 4.** First hydrogenation at room temperature under 1500 kPa of hydrogen of samples after various HPT turns.

Figure 5 shows the first dehydrogenation of samples HPT0, HPT3 and HPT5. Due to uncontrolled experimental conditions, the HPT1 desorption was not registered. For all experiments, the final pressure was around 25 kPa. We observed that the desorption is complete for all samples and that the kinetic is practically the same. This confirms what was observed in our previous investigation: that the effect of mechanical deformation is observed only for the first hydrogenation [16].
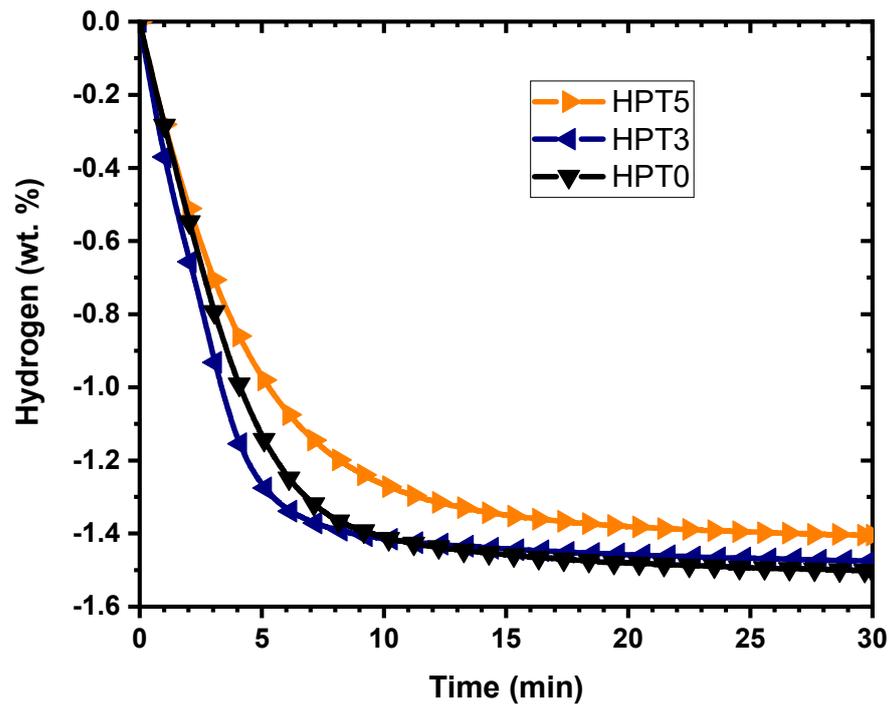
**Figure 5.** First dehydrogenation at room temperature under partial vacuum of HPT samples.

### 3.3. Crystal Structure after Hydrogenation/Dehydrogenation

Figure 6 shows the diffraction patterns of the HPT alloys after one hydrogenation/dehydrogenation cycle. As a comparison, the raw powder ($p < 0.5$) after cycling is also included in the Figure. The structure parameters estimated from Rietveld refinements are shown in Table 2.



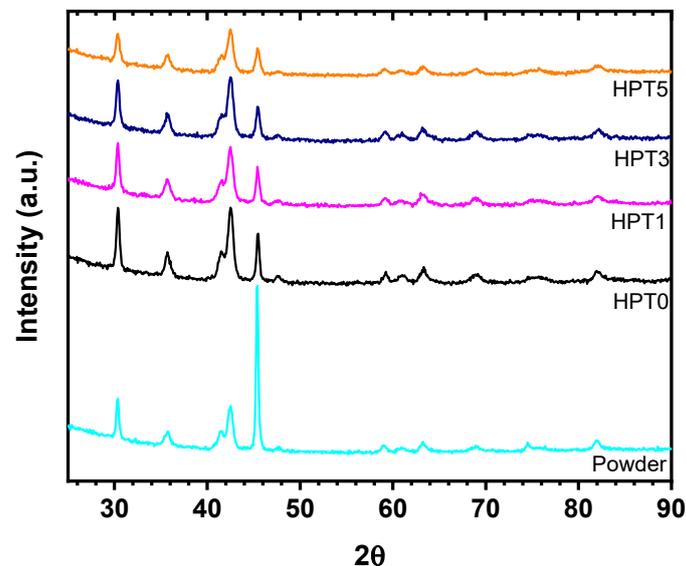**Figure 6.** X-ray diffraction patterns of LaNi$_5$ at various stages: as-received powder (Powder), pressed pellet (HPT0) and pellet after 1, 3 and 5 HPT turns (HPT1, HPT3 and HPT5). The vertical lines indicate the position of LaNi$_5$ Bragg peaks.

**Table 2.** Results of Rietveld refinements of the patterns displayed in Figure 5. *a* and *c* are the lattice parameters of LaNi$_5$ unit cell (space group P6/mmm). Vol is the unit cell volume $\tau$ is the crystallite size and $\varepsilon$ is the microstrain. Error on the last significant digit is indicated in parentheses.

| Sample | *a* (Å) | *c* (Å) | Vol (Å$^3$) | $\tau$ (nm) | $\varepsilon$ (%) |
|---|---|---|---|---|---|
| Powder | 5.027 (1) | 4.0007 (7) | 87.55 (4) | 27 (1) | – |
| HPT0 | 5.016 (1) | 3.986 (1) | 86.84 (6) | 20 (2) | 0.22 (1) |
| HPT1 | 5.017 (2) | 3.985 (1) | 86.85 (6) | 18 (1) | 0.22 (1) |
| HPT3 | 5.017 (1) | 3.986 (1) | 86.86 (6) | 19 (1) | 0.24 (1) |
| HPT5 | 5.018 (2) | 3.986 (1) | 86.93 (7) | 18 (1) | 0.25 (1) |

The raw powder pattern shows LaNi$_5$ single phase with a (002) preferred orientation along a peak at 45.2°. This preferred orientation is probably due to the shape of the particles. It seems that HPT breaks these particles and makes them more randomly oriented. However, this seems counterintuitive, and more detailed experiments are needed to confirm this assertion. Compared to the as-received power (Table 1), the lattice parameters and unit cell volume are slightly bigger and the crystallite size marginally smaller. The bigger unit cell may be due to a small amount of hydrogen still in solid solution in the crystal structure. Lynch and Reilly reported that the variation of the unit cell volume with the hydrogen content in LaNi$_5$H$_x$ for x < 0.17 is approximately linear [33], extrapolating their curve to our measured expansion of the cell volume between as-cast and dehydrogenated state (0.7 Å$^3$), we get x = 0.25 (LaNi$_5$H$_{2.5}$). This also agrees with the Peisl estimation that one hydrogen atom occupies a volume of 2.9 Å$^3$ [34]. This amount of hydrogen corresponds to a capacity of 0.05 wt.%, which is too small to be accurately measured using our Sieverts-type apparatus.

## 4. Discussion

The effects of particle size and high-pressure torsion (HPT) on the hydrogen sorption behavior of LaNi$_5$ were investigated. We found that HPT leads to the reduction of the crystallite size, but most of the effect was due to the first turn. There was an important increase of microstrains at the fifth turn, and it was accompanied by the appearance of a new Bragg peaks.

The investigation of the effect of particle size on the hydrogenation behavior showed that small particles have a longer incubation time and slightly reduced hydrogen capacity compared to the bigger particles. This behavior may be attributed to the presence of an oxide layer, but more tests are needed before a clear mechanism can be proposed. After the first hydrogenation, the dehydrogenation and subsequent hydrogenation were identical for all particle sizes. Thus, particle size has an effect only for the first hydrogenation.

A drastic reduction of incubation time was seen for the HPT's samples, but most of the reduction came from the first HPT turn. Further HPT turns only marginally reduced the incubation time, but there was no loss of hydrogen capacity with the number of turns. The dehydrogenation kinetics were similar for all number of turns and identical to the kinetics of loose powder. This means that, as with particle size, the effect of HPT is seen only on the first hydrogenation.

In a previous investigation, we have seen that cold rolling also enhances the kinetics of the first hydrogenation of LaNi$_5$ [16]. It seems that cold rolling is more efficient in reducing the incubation time of the first hydrogenation, but the total capacity was reduced. A sample cold rolled once in air shows an incubation period of about 3 min. This is almost one order of magnitude shorter than the sample HPT5. However, the capacity of the cold rolled sample was measured to be 1.4 wt.%, which is smaller than the HPT1 capacity. The differences between the two techniques may be explained by the fact that the cold rolled samples are probably more porous than the HPT ones. However, a more systematic investigation is needed to clearly determine the factors that are responsible for the differences in kinetics and capacity.

This investigation showed that HPT and particle size have an effect on only the incubation time of the first hydrogenation of LaNi$_5$. The reasons for such a behavior are still unclear. Nanocrystallinity has a beneficial effect, but there are other properties that play a role. A detailed investigation of the surface by TEM can probably bring crucial knowledge of an incubation mechanism.

**Author Contributions:** Conceptualization, J.H. and J.I.; methodology, J.H. and J.I.; validation, J.I., N.K., R.B.S. and J.H.; formal analysis, J.H. and N.K.; investigation, R.B.S.; resources, J.H. and J.I.; data curation, J.H.; writing—original draft preparation, J.H. and N.K.; writing—review and editing, J.I., N.K., R.B.S. and J.H.; supervision, J.H.; project administration, J.H. and J.I.; funding acquisition, J.H. and J.I. All authors have read and agreed to the published version of the manuscript.

**Institutional Review Board Statement:** Not applicable.

**Informed Consent Statement:** Not applicable.

**Data Availability Statement:** The data presented in this study are available on request from the corresponding author.

**Conflicts of Interest:** The authors declare no conflict of interest.

## References

1. Baran, A.; Polański, M. Magnesium-based materials for hydrogen storage—A scope review. *Materials* **2020**, *13*, 3993. [CrossRef]
2. Kusadome, Y.; Ikeda, K.; Nakamori, Y.; Orimo, S.; Horita, Z. Hydrogen storage capability of MgNi$_2$ processed by high pressure torsion. *Scr. Mater.* **2007**, *57*, 751–753. [CrossRef]
3. Lima, G.F.; Jorge, A.M.; Leiva, D.R.; Kiminami, C.S.; Bolfarini, C.; Botta, W.J. Severe plastic deformation of Mg-Fe powders to produce bulk hydrides. *J. Phys. Conf. Ser.* **2009**, *144*, 012015. [CrossRef]
4. Révész, A.; Kánya, Z.; Verebélyi, T.; Szabó, P.J.; Zhilyaev, A.P.; Spassov, T. The effect of high-pressure torsion on the microstructure and hydrogen absorption kinetics of ball-milled Mg$_{70}$Ni$_{30}$. *J. Alloys Compd.* **2010**, *504*, 83–88. [CrossRef]
5. Edalati, K.; Yamamoto, A.; Horita, Z.; Ishihara, T. High-pressure torsion of pure magnesium: Evolution of mechanical properties, microstructures and hydrogen storage capacity with equivalent strain. *Scr. Mater.* **2011**, *64*, 880–883. [CrossRef]
6. Gómez, E.I.L.; Edalati, K.; Coimbrão, D.D.; Antiqueira, F.J.; Zepon, G.; Cubero-Sesin, J.M.; Botta, W.J. FCC phase formation in immiscible Mg-Hf (magnesium-hafnium) system by high-pressure torsion. *AIP Adv.* **2020**, *10*, 055222. [CrossRef]
7. Dematteis, E.M.; Dreistadt, D.M.; Capurso, G.; Jepsen, J.; Cuevas, F.; Latroche, M. Fundamental hydrogen storage properties of TiFe-alloy with partial substitution of Fe by Ti and Mn. *J. Alloys Compd.* **2021**, *874*, 159925. [CrossRef]
8. Lys, A.; Fadonougbo, J.O.; Faisal, M.; Suh, J.-Y.; Lee, Y.-S.; Shim, J.-H.; Park, J.; Cho, Y.W. Enhancing the Hydrogen Storage Properties of AxBy Intermetallic Compounds by Partial Substitution: A Short Review. *Hydrogen* **2020**, *1*, 38–64. [CrossRef]
9. Hirscher, M.; Yartys, V.A.; Baricco, M.; Bellosta von Colbe, J.; Blanchard, D.; Bowman, R.C.; Broom, D.P.; Buckley, C.E.; Chang, F.; Chen, P.; et al. Materials for hydrogen-based energy storage—Past, recent progress and future outlook. *J. Alloys Compd.* **2020**, *827*, 153548. [CrossRef]
10. Edalati, K.; Matsuda, J.; Arita, M.; Daio, T.; Akiba, E.; Horita, Z. Mechanism of activation of TiFe intermetallics for hydrogen storage by severe plastic deformation using high-pressure torsion. *Appl. Phys. Lett.* **2013**, *103*, 143902. [CrossRef]
11. Edalati, K.; Matsuda, J.; Iwaoka, H.; Toh, S.; Akiba, E.; Horita, Z. High-pressure torsion of TiFe intermetallics for activation of hydrogen storage at room temperature with heterogeneous nanostructure. *Int. J. Hydrogen Energy* **2013**, *38*, 4622–4627. [CrossRef]
12. Edalati, K.; Matsuda, J.; Yanagida, A.; Akiba, E.; Horita, Z. Activation of TiFe for hydrogen storage by plastic deformation using groove rolling and high-pressure torsion: Similarities and differences. *Int. J. Hydrogen Energy* **2014**, *39*, 15589–15594. [CrossRef]
13. Gómez, E.I.L.; Edalati, K.; Antiqueira, F.J.; Coimbrão, D.D.; Zepon, G.; Leiva, D.R.; Ishikawa, T.T.; Cubero-Sesin, J.M.; Botta, W.J. Synthesis of Nanostructured TiFe Hydrogen Storage Material by Mechanical Alloying via High-Pressure Torsion. *Adv. Eng. Mater.* **2020**, *22*, 1–6. [CrossRef]
14. Broom, D.P. *Hydrogen Storage Materials*, 1st ed.; Springer: London, UK, 2011; ISBN 978-0-85729-220-9.
15. Corré, S.; Bououdina, M.; Kuriyama, N.; Fruchart, D.; Adachi, G.Y. Effects of mechanical grinding on the hydrogen storage and electrochemical properties of LaNi$_5$. *J. Alloys Compd.* **1999**, *292*, 166–173. [CrossRef]
16. Tousignant, M.; Huot, J. Hydrogen sorption enhancement in cold rolled LaNi$_5$. *J. Alloys Compd.* **2014**, *595*, 22–27. [CrossRef]
17. Zhilyaev, A.P.; Langdon, T.G. Using high-pressure torsion for metal processing: Fundamentals and applications. *Prog. Mater. Sci.* **2008**, *53*, 893–979. [CrossRef]
18. Bridgman, P.W. Effects of high shearing stress combined with high hydrostatic pressure. *Phys. Rev.* **1935**, *48*, 825–847. [CrossRef]
19. Edalati, K.; Shao, H.; Emami, H.; Iwaoka, H.; Akiba, E.; Horita, Z. Activation of titanium-vanadium alloy for hydrogen storage by introduction of nanograins and edge dislocations using high-pressure torsion. *Int. J. Hydrogen Energy* **2016**, *41*, 8917–8924. [CrossRef]

20. Edalati, K.; Akiba, E.; Horita, Z. High-pressure torsion for new hydrogen storage materials. *Sci. Technol. Adv. Mater.* **2018**, *19*, 185–193. [CrossRef]

21. Yamamoto, T.; Inui, H.; Yamaguchi, M. Deformation of LaNi$_5$ by uniaxial compression and hydrogenation. *Intermetallics* **2001**, *9*, 987–991. [CrossRef]

22. Balzar, D.; Audebrand, N.; Daymond, M.R.; Fitch, A.; Hewat, A.; Langford, J.I.; Le Bail, A.; Louër, D.; Masson, O.; McCowan, C.N.; et al. Size-strain line-broadening analysis of the ceria round-robin sample. *J. Appl. Crystallogr.* **2004**, *37*, 911–924. [CrossRef]

23. Joubert, J.M.; Paul-Boncour, V.; Cuevas, F.; Zhang, J.; Latroche, M. LaNi$_5$ related AB$_5$ compounds: Structure, properties and applications. *J. Alloys Compd.* **2021**, *862*, 158163. [CrossRef]

24. Abolkarlou, M.A.; Amerioun, M.H. Experimental Study of Structural and Magnetic Properties of LaNi$_5$ and MmNi$_{4.7}$Al$_{0.3}$ Hydrogen Storage Alloys. *J. Supercond. Nov. Magn.* **2019**, *32*, 1853–1857. [CrossRef]

25. Wu, E.; Kisi, E.H.; Gray, E.M.A. Modelling Dislocation-Induced Anisotropic Line Broadening in Rietveld Refinements Using a Voigt Function. II. Application to Neutron Powder Diffraction Data. *J. Appl. Crystallogr.* **1998**, *31*, 363–368. [CrossRef]

26. Joseph, B.; Iadecola, A.; Schiavo, B.; Cognigni, A.; Olivi, L.; D'Alì Staiti, G.; Saini, N.L. Local structure of ball-milled LaNi$_5$ hydrogen storage material by Ni K-edge EXAFS. *J. Solid State Chem.* **2010**, *183*, 1550–1554. [CrossRef]

27. Diehm, P.M.; Ágoston, P.; Albe, K. Size-dependent lattice expansion in nanoparticles: Reality or anomaly? *ChemPhysChem* **2012**, *13*, 2443–2454. [CrossRef]

28. Schlapbach, L.; Seiler, A.; Siegmann, H.C.; Waldkirch, T.V.; Zücher, P.; Brundle, C.R. Self restoring of the active surface in LaNi$_5$. *Int. J. Hydrogen Energy* **1979**, *4*, 21–28. [CrossRef]

29. Selvam, P.; Viswanathan, B.; Srinivasan, V. Some comments on modes of activation of LaNi$_5$ and CaNi$_5$ alloys for hydrogen storage. *Int. J. Hydrogen Energy* **1989**, *14*, 687–689. [CrossRef]

30. Selvam, P.; Viswanathan, B.; Swamy, C.S.; Srinivasan, V. Surface properties of LaNi$_5$: A reinvestigation. *Int. J. Hydrogen Energy* **1991**, *16*, 23–33. [CrossRef]

31. Litvinov, V.A.; Okseniuk, I.I.; Shevchenko, D.I.; Bobkov, V.V. Studying the Interaction of LaNi$_5$ Intermetallic Alloy with Oxygen by SIMS. *J. Surf. Investig.* **2020**, *14*, 1358–1365. [CrossRef]

32. Matsuda, J.; Nakamura, Y.; Akiba, E. Lattice defects introduced into LaNi$_5$-based alloys during hydrogen absorption/desorption cycling. *J. Alloys Compd.* **2011**, *509*, 7498–7503. [CrossRef]

33. Lynch, J.F.; Reilly, J.J. Behavior of H-LaNi$_5$ solid solutions. *J. Less-Common Met.* **1982**, *87*, 225–236. [CrossRef]

34. Peisl, H. Lattice strains due to hydrogen in metals. In *Hydrogen in Metals I. Topics in Applied Physics*; Alefeld, G., Völkl, J., Eds.; Springer: Berlin/Heidelberg, Germany, 1978; Volume 28, pp. 53–74. ISBN 978-3-540-35892-3.